

Article

How to Accurately Determine the Ohmic Contact Properties on n-Type 4H-SiC

Clément Berger , Daniel Alquier  and Jean-François Michaud * 

GREMAN UMR-CNRS 7347, Université de Tours, INSA Centre Val de Loire, 16 rue Pierre et Marie Curie, 37071 Tours Cedex 2, France; clement.berger@univ-tours.fr (C.B.); daniel.alquier@univ-tours.fr (D.A.)

* Correspondence: jean-francois.michaud@univ-tours.fr

Abstract: The electrical properties of ohmic contacts are classically investigated by using the transfer length method (TLM). In the literature, the TLM patterns are fabricated onto different substrate configurations, especially directly onto the 4H-SiC wafers. But, due to the high doping level of commercial substrates, the current is not confined close to the contact and, in this case, the specific contact resistance (SCR) value is overestimated. In this article, we propose, by the means of simulations, to investigate the influence of the layer under the contact towards the estimation of the SCR. The simulation results highlight that, for an accurate determination of the SCR values, an isolation layer between the contact and the silicon carbide substrate is mandatory. Thus, we have determined the characteristics (doping level and thickness) of a suitable isolation layer compatible with SCR values ranging from 10^{-3} to $10^{-6} \Omega \cdot \text{cm}^2$.

Keywords: simulation; ohmic contact; electrical characterization; c-TLM; silicon carbide



Citation: Berger, C.; Alquier, D.; Michaud, J.-F. How to Accurately Determine the Ohmic Contact Properties on n-Type 4H-SiC. *Electronics* **2024**, *13*, 217. <https://doi.org/10.3390/electronics13010217>

Academic Editors: Andrei Avram, Ana-Maria Lepadatu, Florin Nastase and Martino Aldrigo

Received: 13 December 2023

Revised: 28 December 2023

Accepted: 29 December 2023

Published: 3 January 2024



Copyright: © 2024 by the authors. Licensee MDPI, Basel, Switzerland. This article is an open access article distributed under the terms and conditions of the Creative Commons Attribution (CC BY) license (<https://creativecommons.org/licenses/by/4.0/>).

1. Introduction

Silicon carbide (SiC) is a wide bandgap semiconductor, able to work under a high temperature and high power. Among the different polytypes, 4H-SiC is well-established in the field of power electronics. This hexagonal polytype presents excellent thermal and electrical properties, which allows to reduce the active 4H-SiC layer to a 10 μm range. As the growth of this active layer must be perfectly controlled, the epitaxy is achieved on the Si-face of 4H-SiC substrates. Therefore, for vertical devices, the ohmic contacts are fabricated onto the substrate backside (C-face). Their fabrication by rapid thermal annealing (RTA) has been deeply studied in the literature during the past decade [1–6]. In the last few years, the improvement of devices has required technical modifications of the device fabrication [7], and laser thermal annealing (LTA) is frequently used to fabricate ohmic contact thanks to the low substrate temperature elevation [8,9]. In addition, several studies have been performed in order to obtain ohmic contacts with good electrical properties consecutive to laser irradiation [10–15].

To investigate the ohmic properties of the contacts, the transfer length method (TLM) is commonly applied [16]. This method allows to determine the specific contact resistance (SCR) (the main parameter to evaluate the electrical contacts' properties) independently of the contact geometry as soon as it fulfils the TLM model. In the literature, ohmic contacts are characterized by different substrate configurations [14,17–19]. Some teams fabricate the TLM structures directly onto the substrate, others use a substrate isolation or grow a highly doped layer onto the substrate.

In this article, by the means of TCAD simulations, we study the role of such configurations and we propose a structure that allows an accurate determination of the electrical properties of ohmic contacts.

2. TLM Model

The circular TLM (c-TLM) method is commonly performed to determine specific contact resistance. The model is detailed in [16]. Contrary to linear patterns, it does not require lateral isolation of its structures, which simplifies the fabrication process.

The c-TLM method uses several circular electrodes, each one having its own spacing, as presented in Figure 1a. If the current–voltage (I–V) characteristics are linear, the contacts are ohmic and the resistance associated to each structure can be extracted. However, due to the circular shape, the resistance has to be corrected to avoid a miscalculation of specific contact resistance. This correction factor C_s is defined by Equation (1), where R_0 is the radius of the inner electrode and s is the c-TLM spacing.

$$C_s = \frac{R_0}{s} \ln \left(1 + \frac{s}{R_0} \right) \tag{1}$$

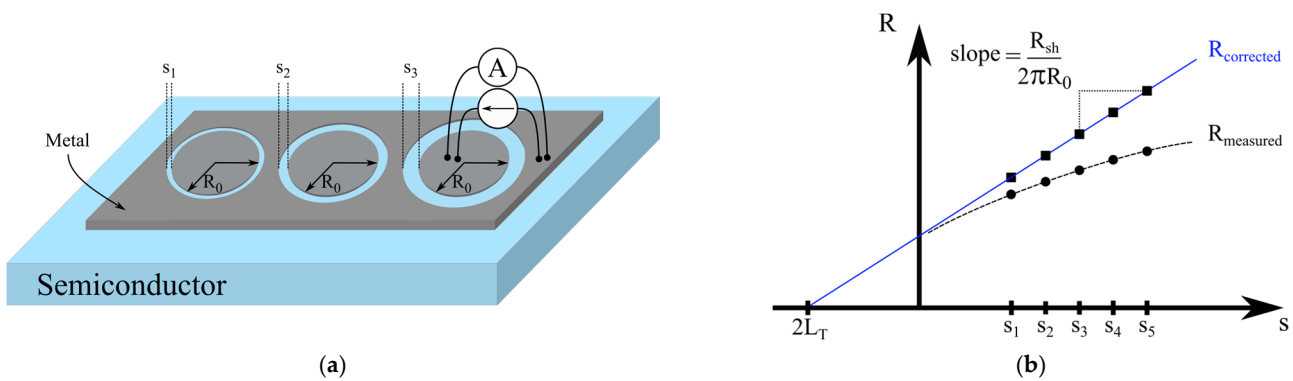


Figure 1. (a) Representation of patterns used for circular c-TLM method. (b) Illustration of the evolution of the resistance as a function of the spacing for an ohmic contact.

Afterwards, the evolution of the resistance as a function of the c-TLM spacing allows to determine the sheet resistance R_{sh} directly under the contacts and the transfer length L_T thanks to Equation (2).

$$R = \frac{R_{sh}}{2\pi R_0} (s + 2L_T) C_s \tag{2}$$

The transfer length is considered the minimal distance required for the current to go through a metal–semiconductor interface. A typical evolution of the resistance is presented in Figure 1b. Finally, the SCR can be calculated by Equation (3).

$$SCR = R_{sh} \times L_T^2 \tag{3}$$

3. Motivations

As mentioned previously, the ohmic contacts were elaborated on the wafer backside directly on the carbon face of a highly doped silicon carbide substrate, for whatever was the method used to obtain the ohmic contact. As a consequence, our preliminary experiments dealing with the elaboration of a titanium ohmic contact with a laser irradiation were performed directly on the SiC substrate. At this time, based on [10], this metal showed promise to form a good ohmic contact on 4H-SiC because it led to the lowest SCR and to a good contact morphology (before nickel demonstrated superior electrical performances and became the reference contact formed by laser annealing a few years later). When we fabricated the titanium contacts directly on the wafer backside by laser annealing, the resistance values measured for the c-TLM patterns were very low.

Figure 2a presents typical I–V characterizations of an annealed titanium contact laser. The curves are linear, which indicates that the contact is ohmic. Nevertheless, by plotting the evolution of the corrected resistance as a function of the spacing, reported in Figure 2b,

we can see that the curve is not strictly linear and has a low correlation coefficient of 0.46. Thus, even if the contacts seem ohmic, it is not possible to reliably determine the specific contact resistance. Moreover, for such low resistance levels, the measuring device resolution can affect the determination of the resistance. In order to understand these results, we decided to simulate the electrical behavior of the c-TLM structures.

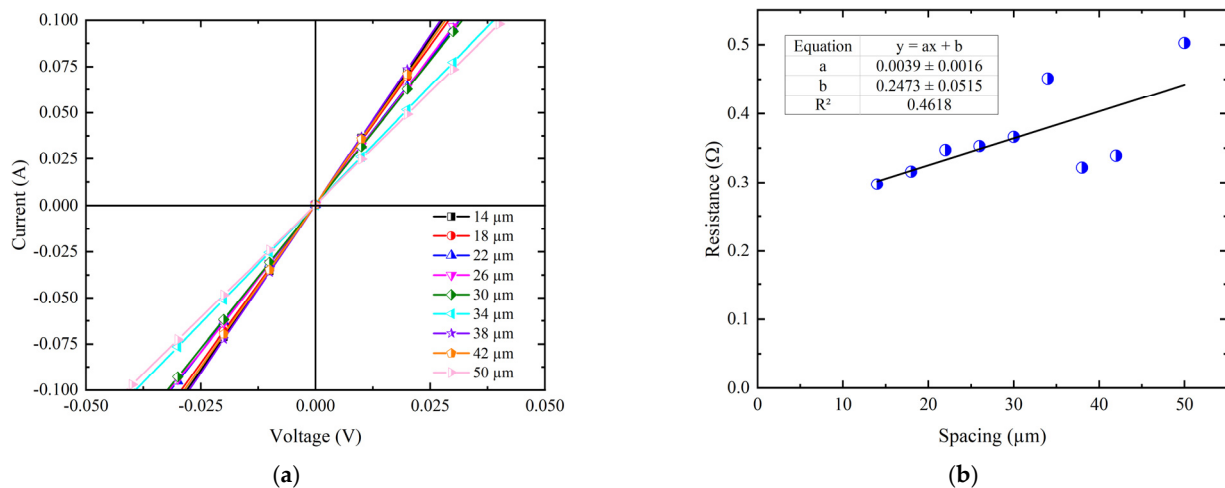


Figure 2. (a) I-V characteristics measured for a c-TLM pattern with spacings ranging from 12 to 48 μm for an annealed Ti/4H-SiC contact laser. (b) Evolution of the corrected resistance as a function of the spacing for the Ti/4H-SiC contacts.

3.1. Simulations of c-TLM Structures onto 350 μm-Thick 4H-SiC Substrate

The configuration used to determine the specific contact resistance of our laser irradiated samples was simulated by the means of TCAD Sentaurus Device software developed by Synopsys. The physics models involved in the simulation of the c-TLM electrical behavior were taken from the software library, e.g., the thermionic model, the Fermi model, the incomplete ionization, and the Shockley–Read–Hall recombination model. We reproduced a c-TLM pattern, presented in Figure 3a, composed of the 200 μm wide circular inner electrode separated from the surrounding outer electrode by a distance of 48 μm. The contact was defined only by its specific contact resistance value, fixed at $1 \times 10^{-5} \Omega \cdot \text{cm}^2$, that corresponded to good ohmic properties on n-type 4H-SiC. The contacts were deposited directly onto a 350 μm thick 4H-SiC substrate doped with a nitrogen concentration of $1 \times 10^{18} \text{ at} \cdot \text{cm}^{-3}$ that corresponded approximately to the resistivity of commercial wafers ($20 \text{ m}\Omega \cdot \text{cm}$). Figure 3b represents a 3D view of the current density distribution of the structure for a difference of potential of 1 V applied between the inner and the outer electrode. A cross-sectional view extracted from this image is presented in Figure 3c. From this image, we can see that the electrons flowed mainly between the electrodes, but a non-negligible part of it circulated deeply in the substrate. As a result, this current circulation is not in agreement with the TLM model, which supposes that the charge carriers flow near to the contacts. In Figure 3d, we simulated the I-V curves for several spacings from 12 to 48 μm to determine their resistances. The curves were quite superposed, which suggests similar resistance values. The resistances, after applying the correction factor presented in Equation (1), are presented in Figure 3e. For spacing between the contacts ranging from 12 to 48 μm, the simulated resistances varied between 150 and 180 mΩ. These simulation results are in good agreement with the experimental values that we found. Moreover, measuring such low resistances is challenging and can lead to difficulties in discriminating the resistance variations with the spacing on classical 4H-SiC substrates.

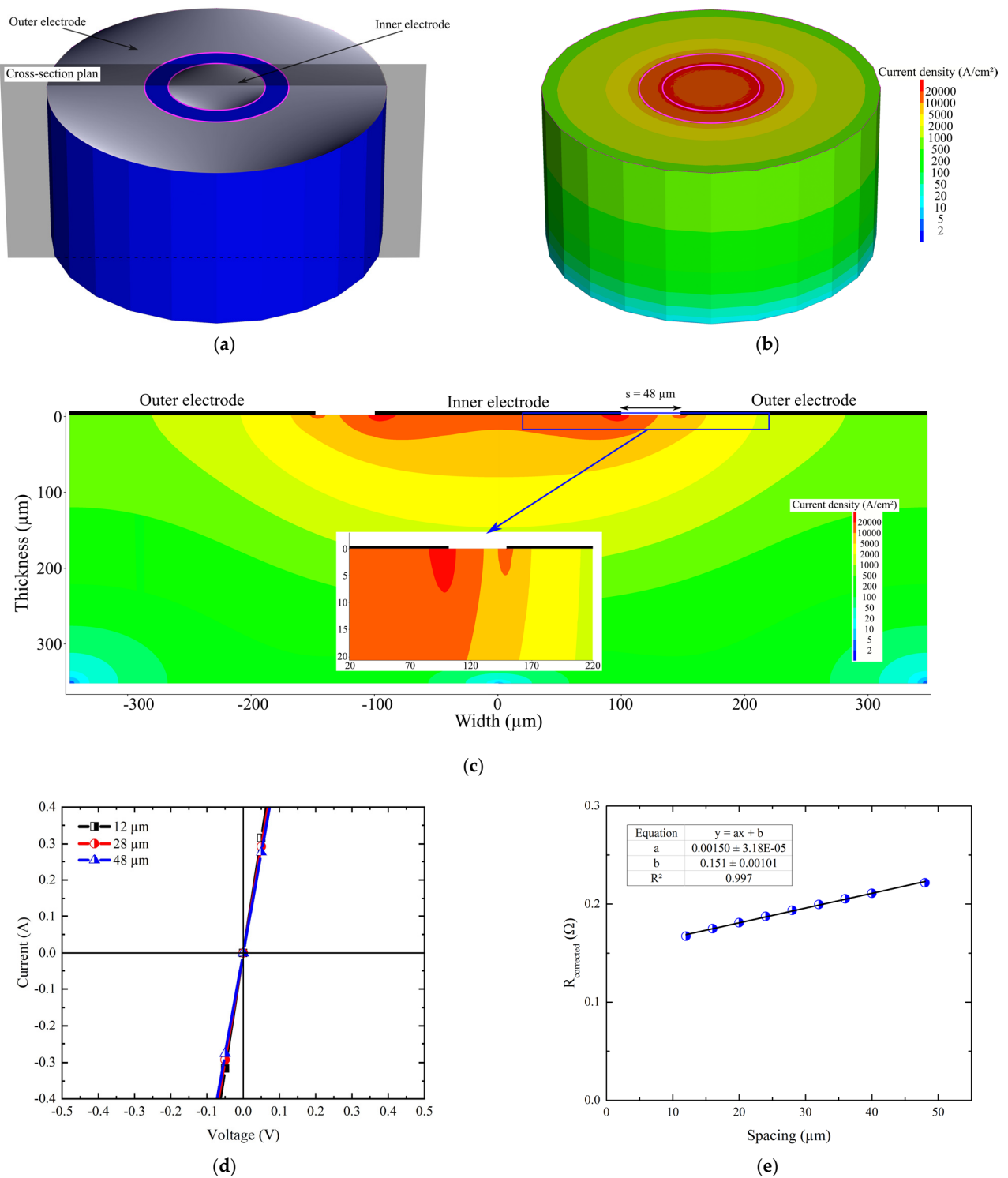


Figure 3. (a) A 3D view of the simulated structure; the specific contact resistance at the electrode/4H-SiC interface is fixed at $1 \times 10^{-5} \Omega \cdot \text{cm}^2$. Current density circulating into a c-TLM structure deposited directly onto the substrate under a difference of potential of 1 V in (b) 3D view and (c) cross-sectional view. In (c), an inset picture is presented, highlighting the current density between the electrodes. (d) Simulated I-V characteristics for several c-TLM spacings. (e) Evolution of the resistance as a function of the c-TLM spacing.

The metal deposited on the silicon carbide substrate led to the structure presented in Figure 4. The measured resistance, determined from I-V measurements, corresponded to

the contribution of the different resistances that hampered the current to circulate: the metal resistance R_m , the contact resistance R_C , and the sheet resistance of the semiconductor layer just under the metal R_{sh} . When the metal was directly deposited on SiC substrates, as shown in Figure 3c, the current flowed deeply into the substrate. Therefore, as far as the SiC substrate thickness increased, the R_{sh} resistance was reduced and consequently the total resistance (becoming sufficiently low enough to not be precisely measured).

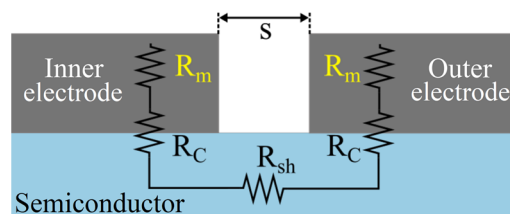


Figure 4. Representation of the main contributions to the resistance measured in a metal–semiconductor structure.

These simulation results seem to explain the difficulties encountered with our preliminary experiments on a thick SiC substrate. To confirm this behavior, we decided to perform the same simulations but considering a thin substrate.

3.2. Simulations of c-TLM Structures onto 2 μm Thick 4H-SiC Substrate

Based on the previous simulation results, we performed additional simulations using an arbitrary 2 μm thick 4H-SiC substrate. The idea was to try to confine the current circulation near the electrodes. In Figure 5a, we can see that the simulated I-V curves were well differentiable, contrary to the ones obtained with a classical 350 μm thick 4H-SiC substrate (see Figure 3d). Their associated resistances, reported in Figure 5b, evolved in the range of 1.3 to 3.5 Ω , which would be convenient to characterize. Obviously, experimentally processing a 2 μm thick SiC substrate is impossible. But, the simulation results highlight the large benefits coming from the confinement of the current just underneath the contact to accurately characterize the electrical properties of the contacts.

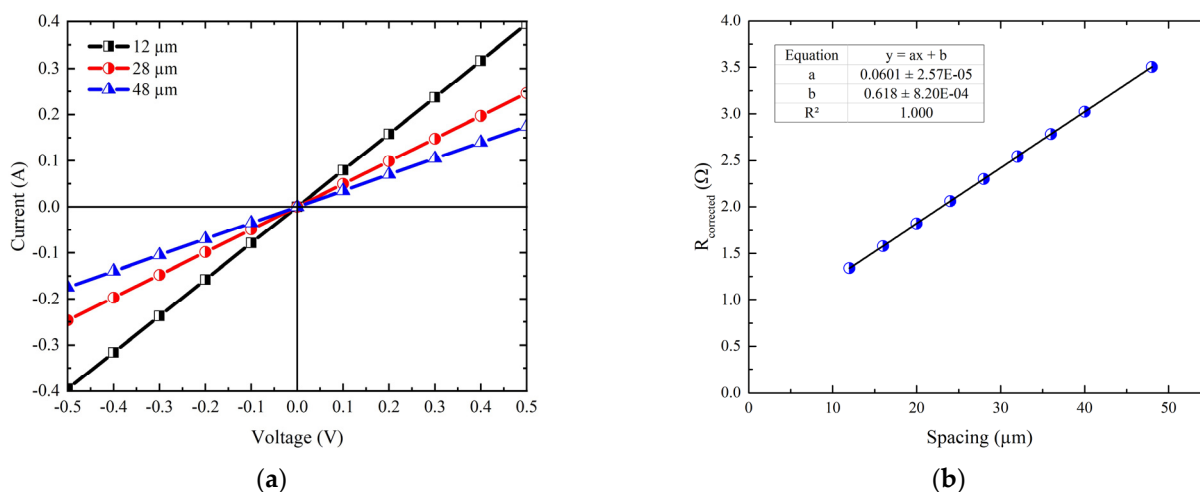


Figure 5. (a) Simulated I-V characteristics for several c-TLM spacings fabricated on a 2 μm thick substrate with the specific contact resistance equal to $1 \times 10^{-5} \Omega \cdot \text{cm}^2$. (b) Evolution of the resistance as a function of the c-TLM spacing.

The confinement of the current close to the contact can be obtained in two different ways. The first one is to drastically increase the 4H-SiC resistivity by decreasing the doping level. Nevertheless, ohmic contacts are generally fabricated directly on bulk wafers, i.e., on 4H-SiC doped in the range of $1 \times 10^{18} \text{ at} \cdot \text{cm}^{-3}$, as configured in our simulations.

Moreover, a high doping level helps to obtain a good ohmic contact on 4H-SiC [20] and, as the conduction mechanisms through a metal–semiconductor interface are sensible to the doping, it seems relevant to study structures close to the commercial wafer [21,22]. As a low doped substrate is not convenient to obtain an ohmic contact, we used a second way to confine the current that uses a low doped SiC film to act as an isolation layer and a 2 μm thick highly doped SiC film compatible with the ohmic contact achievement. Experimentally, these two layers can be grown by epitaxy. Aluminum implantation could also be an interesting solution to define the isolation layer, but this process induces defects that cannot be fully recovered even consecutively to a high annealing temperature of 1600 $^{\circ}\text{C}$ [23,24]. As epitaxy on 4H-SiC becomes more and more mastered, it seems useable to fulfil our objectives [17,25]. The only drawback could be the fact that, as epitaxy is not yet controlled on the C-face, both layers have to be grown onto the Si-face, whereas the ohmic contacts are elaborated on the C-face for the commercial devices.

3.3. Simulations of *c*-TLM Structures with an Electrical Isolation of the 4H-SiC Substrate

To investigate the role of the isolation layer, we simulated the structure composed of a low doped nitrogen layer ($10\ \mu\text{m}/1 \times 10^{16}\ \text{at}\cdot\text{cm}^{-3}$) grown onto a classical 4H-SiC substrate ($350\ \mu\text{m}/1 \times 10^{18}\ \text{at}\cdot\text{cm}^{-3}$). Such a doping level is well-controlled and, to our knowledge, is the standard doping level for the drift layer grown in 4H-SiC devices. Above this isolation layer, a thin n^+ layer ($2\ \mu\text{m}/1 \times 10^{18}\ \text{at}\cdot\text{cm}^{-3}$) was grown. The schematic representation of the structure's cross-section, for a specific contact resistance fixed at $1 \times 10^{-5}\ \Omega\cdot\text{cm}^2$, is presented in Figure 6a. Figure 6b shows the current density under a difference of potential of 1 V between electrodes in the 3D structure. To better reveal the current circulation in the *c*-TLM structure, a cross-section was extracted from the 3D view and is presented in Figure 6c. In this configuration, it can be clearly seen that the current was mostly confined to the n^+ top layer, which demonstrates the efficiency of the n^- layer to prevent the current to circulate deeply in the substrate. Figure 6d presents the simulated I-V characteristics for several *c*-TLM spacings. Similar to the structure composed of only 2 μm thick 4H-SiC, I-V curves for each spacing were clearly differentiated. Figure 6e reports the resistance associated to each spacing. Their values varied between 0.8 and 1.2 Ω , which seemed high enough to be measured. Nevertheless, we can see that this variation range (0.8–1.2 Ω) was not exactly similar to the one obtained for the 2 μm thick 4H-SiC substrate (1.3–3.5 Ω) reported in Figure 5b. Since the difference between those configurations is the presence of an isolation layer under the 2 μm thick highly doped layer, we can reasonably suppose that the resistance difference comes from this non-ideal isolation. Therefore, as this isolation layer impacts the electrical characteristics of the contacts, that means the determination of the SCR values and a deep investigation of the influence of this layer seems essential. This is the main objective of this contribution.

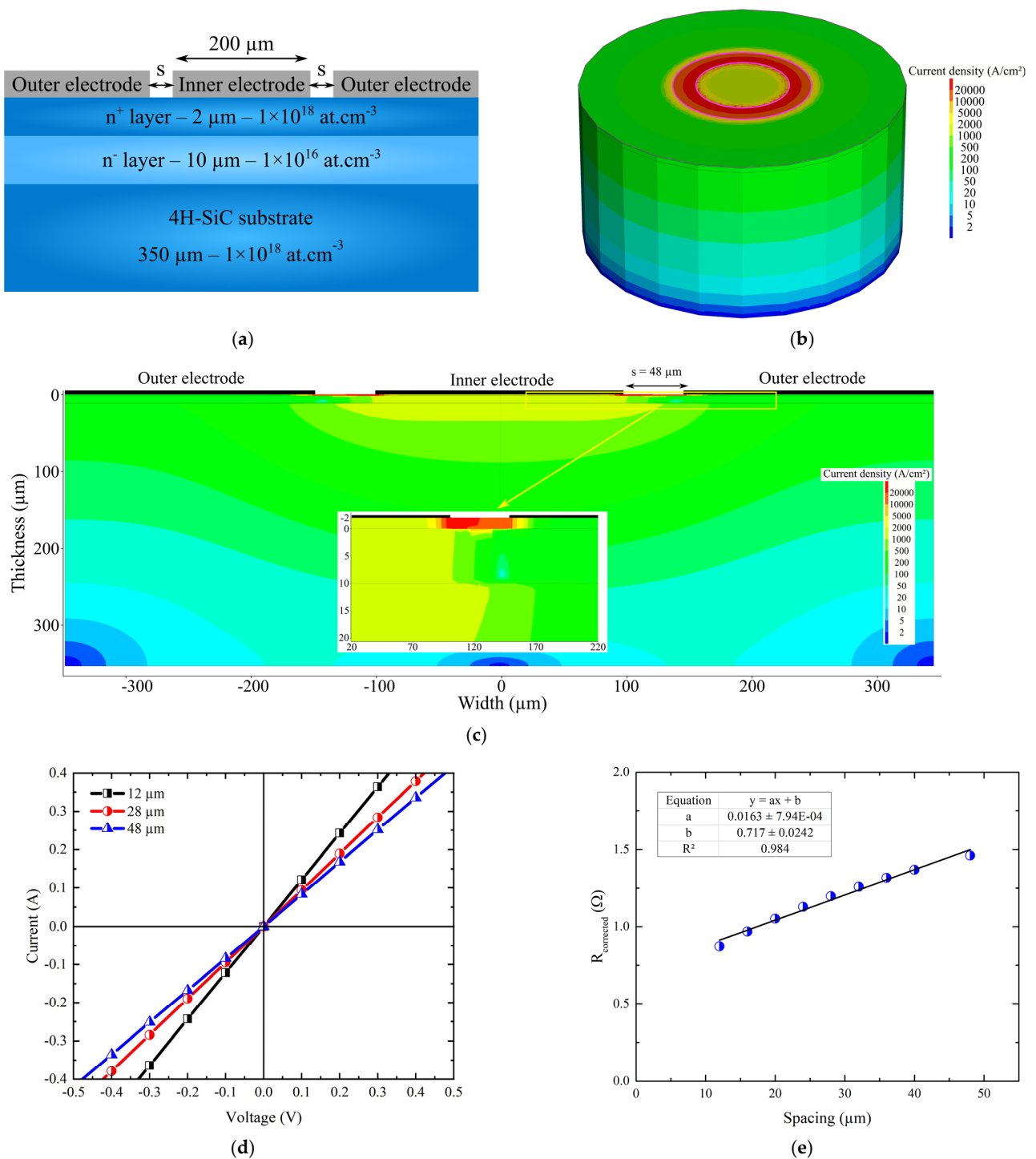


Figure 6. (a) Diagram of the structure with the isolation layer ($10\ \mu\text{m}/1 \times 10^{16}\ \text{at}\cdot\text{cm}^{-3}$); the specific contact resistance at the electrode/4H-SiC interface is fixed at $1 \times 10^{-5}\ \Omega\cdot\text{cm}^2$. Simulated current density circulating in a c-TLM structure ($s = 48\ \mu\text{m}$) under a difference of potential of 1 V in (b) 3D view and (c) cross-sectional view. In (c), an inset picture is presented, highlighting the current density between the electrodes. (d) Simulated I-V characteristics for several spacings of the c-TLM with their associated resistance. (e) Evolution of the resistance of a function of the spacing.

4. Design and Methods

The method used to estimate the influence of the isolation is described in Figure 7. The approach began with the definition of the c-TLM structure. On the 4H-SiC substrate ($350\ \mu\text{m}/1 \times 10^{18}\ \text{at}\cdot\text{cm}^{-3}$) was deposited the n^- isolation layer, with variable characteris-

tics in terms of thickness (1–40 μm) and doping level (5×10^{13} – 1×10^{16} $\text{at}\cdot\text{cm}^{-3}$). Then, the n^+ layer, presenting a doping level equivalent to the SiC substrates (1×10^{18} $\text{at}\cdot\text{cm}^{-3}$), was grown onto the n^- layer. The influence of its thickness is investigated in Section 5.1. To complete the structure definition, the inner and the outer electrodes, distant by a spacing s , were placed at the top of the n^+ layer. To optimize the calculation resources, only half of the cross-section was design and meshed. The contact electrical performances were defined by their specific contact resistance ($\text{SCR}_{\text{fixed}}$) ranging from 1×10^{-3} $\Omega\cdot\text{cm}^2$ to 1×10^{-6} $\Omega\cdot\text{cm}^2$. Then, the current circulation was calculated for the rebuilt 3D structure by a cylindrical symmetry along the thickness axis, for voltage ranging from -1 V to 1 V to simulate the I-V curve. The described approach was repeated for each spacing from 12 to 48 μm . As a result, nine I-V characteristics were simulated as performed experimentally.

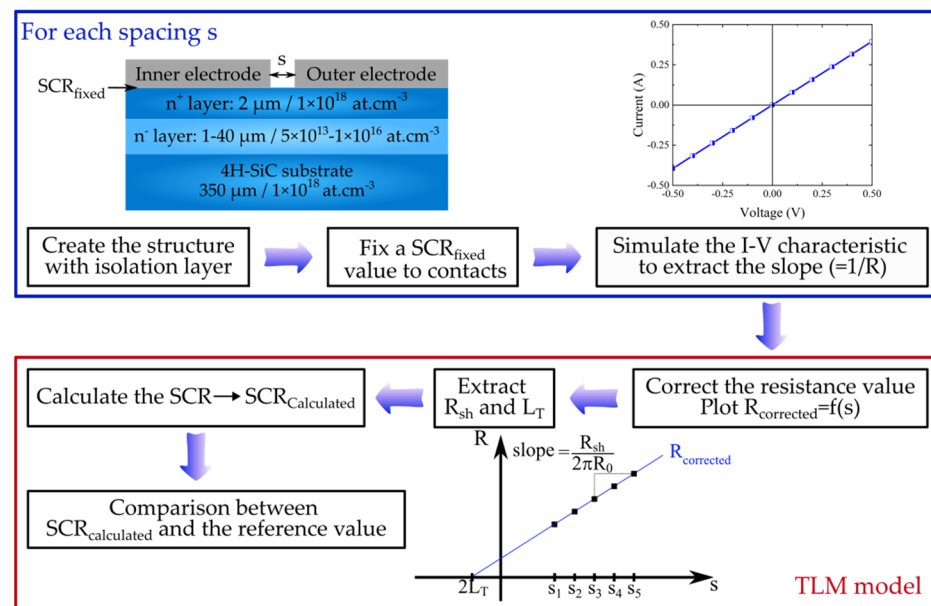


Figure 7. Schematic representation of the method used to determine the $\text{SCR}_{\text{calculated}}$. The reference SCR value is obtained with the 2 μm thick n^+ layer, as discussed in Section 5.1.

Finally, the classical c-TLM procedure was applied to determine the specific contact resistance. From the linear I-V curves, the resistance associated to each spacing was extracted. After applying a correction factor to the resistance, depending on the c-TLM spacing, the evolution of the corrected resistance was plotted as a function of the spacing. A linear fitting was used to extract the sheet resistance R_{sh} and the transfer length L_T , as presented in Figure 1b. Finally, the specific contact resistance, $\text{SCR}_{\text{calculated}}$, was determined based on Equation (3). According to the isolation layer properties, the current could flow through this region and circulate into the substrate. If the isolation was not appropriate, it could lead to an $\text{SCR}_{\text{calculated}}$ that deviated from the $\text{SCR}_{\text{fixed}}$. As a consequence, thanks to this method, the influence of the isolation layer parameters (thickness/doping level) could be evaluated, as presented in the next section.

5. Simulation Results

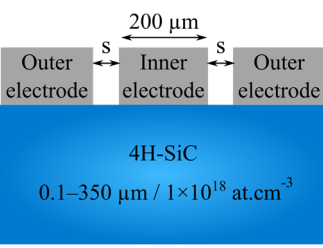
In this section, prior to focusing on isolated structures, we propose to investigate the impact of the n^+ layer on the calculation of the SCR to fix its thickness for the following simulations involving the isolation layer.

5.1. Influence of the Layer Thickness Underneath the Electrodes on the SCR Determination

Table 1 presents the specific contact resistance calculated ($\text{SCR}_{\text{calculated}}$) for several thicknesses of the n^+ layer and for several fixed specific contact resistances to the interface electrode/4H-SiC ($\text{SCR}_{\text{fixed}}$). First, no matter the $\text{SCR}_{\text{fixed}}$, the thickness reduction of the

n^+ layer lowers the determination of the specific contact resistance $SCR_{calculated}$, which confirms that this layer affects the SCR. The thickest n^+ layer (350 μm) always overestimates the specific contact resistance ($SCR_{calculated} > SCR_{fixed}$). On the other side, the thinnest one always underestimates it a bit. Secondly, we see that in almost all conditions, no matter the 4H-SiC thickness or the contact performances, the $SCR_{calculated}$ never exactly equals the SCR_{fixed} . Therefore, there is no ideal n^+ layer allowing to perfectly determine the electrical contact properties for the whole range of SCR_{fixed} ; an error is always committed due to the n^+ layer thickness. Thirdly, the largest deviations occur for the thickest 4H-SiC layer and for the best ohmic contact at $SCR_{fixed} = 10^{-6} \Omega \cdot cm^2$. For this SCR_{fixed} value, the thinnest layers (0.1 and 0.5 μm) generate the lowest error, around 4%, while it increases to 14%, 31%, 84%, and 162% for thicknesses of 1 μm , 2 μm , 5 μm , and 10 μm , respectively. It means that the ohmic contact properties' improvement that corresponds to a decrease in the SCR_{fixed} value requires a better current confinement, illustrated by the reduction in the n^+ thickness. For the other SCR_{fixed} from $10^{-3} \Omega \cdot cm^2$ to $10^{-5} \Omega \cdot cm^2$, the error on the $SCR_{calculated}$ is lower than 5% for layers ranging from 0.5 to 2 μm , which seems sustainable to accurately quantify the ohmic contact properties.

Table 1. Simulated specific contact resistance for several 4H-SiC thicknesses. The symbol “ Δ ” indicates that the transfer length is higher than a quarter of the inner electrode radius ($L_T > 25 \mu m$).



4H-SiC thickness (μm)	SCR_{fixed}			
	$10^{-3} \Omega \cdot cm^2$	$10^{-4} \Omega \cdot cm^2$	$10^{-5} \Omega \cdot cm^2$	$10^{-6} \Omega \cdot cm^2$
350	1.41 Δ	1.49 Δ	2.38 Δ	9.99 Δ
10	1.20 Δ	1.01 Δ	1.16	2.62
5	1.12 Δ	0.98	1.06	1.84
2	1.03 Δ	0.97	1.00	1.31
1	0.99 Δ	0.96	0.97	1.14
0.5	0.97	0.96	0.96	1.04
0.1	0.96	0.95	0.93	0.96

We note that, in some cases, the transfer length extracted from c-TLM simulations is high, especially for $SCR_{fixed} = 10^{-3} \Omega \cdot cm^2$. The transfer length is representative of the minimal distance needed by the current to go through the interface. If this parameter is in the same range as the electrodes' dimensions, a miscalculation of the SCR is committed. Therefore, it is considered that it should be a few times lower than the inner electrode radius [26].

These results indicate that the thickness of 0.5 μm seems to give the $SCR_{calculated}$ values the closest to the SCR_{fixed} . Nevertheless, in this field of research dealing with the ohmic contacts fabricated using laser annealing, the c-TLM patterns are fabricated after laser irradiation by the means of dry etching [11,27]. Since the ohmic contact consumes SiC during the annealing, the etching of the c-TLM spacing has to remove some 4H-SiC thickness to ensure that the contact is fully removed. Then, the over-etch of this layer at the c-TLM spacing could generate a current crowding, thus affecting the electrical measurements. Considering those points, it might be tricky to process a 0.5 μm thick 4H-SiC layer with such a process. Therefore, for the simulation of the isolated structures, we fix the n^+ layer thickness to 2 μm , even if it does not bring the most accurate results for SCR_{fixed} of $10^{-6} \Omega \cdot cm^2$. In our conditions, as the stand-alone 2 μm thick n^+ layer represents the ideal current confinement, the SCR values presented in Table 1 for this thickness are considered as the reference (SCR_{ref}) for the next study dealing with the influence of the isolation layer.

5.2. Influence of the Isolation Layer on the SCR Determination

Up to now, we completely defined the n^+ layer ($2 \mu\text{m}/1 \times 10^{18} \text{ at}\cdot\text{cm}^{-3}$) and the bulk substrate ($350 \mu\text{m}/1 \times 10^{18} \text{ at}\cdot\text{cm}^{-3}$) parameters. Then, we proposed to study the effect of the isolation characteristics on the SCR determination. To do so, we varied the thickness (from 1 to $40 \mu\text{m}$) and doping level (from 5×10^{13} to $1 \times 10^{16} \text{ at}\cdot\text{cm}^{-3}$) of the n^- layer (see Figure 7). The calculated SCR values are presented in Table 2.

To highlight the results of Table 2, for better visualization, we also present the $\text{SCR}_{\text{calculated}}$ values in chart view for the highest and the lowest doped isolation layers in Figure 8. These graphs report the evolution of the calculated specific contact resistance as a function of the thickness of the isolation layer for both doping levels. The dashed lines represent the SCR_{ref} values obtained with the $2 \mu\text{m}$ thick layer for each $\text{SCR}_{\text{fixed}}$. Comparison of the isolation layers is achieved thanks to the overestimation factor that is defined by the relation of the calculated specific contact resistance divided by the reference one ($\text{SCR}_{\text{calculated}}/\text{SCR}_{\text{ref}}$).

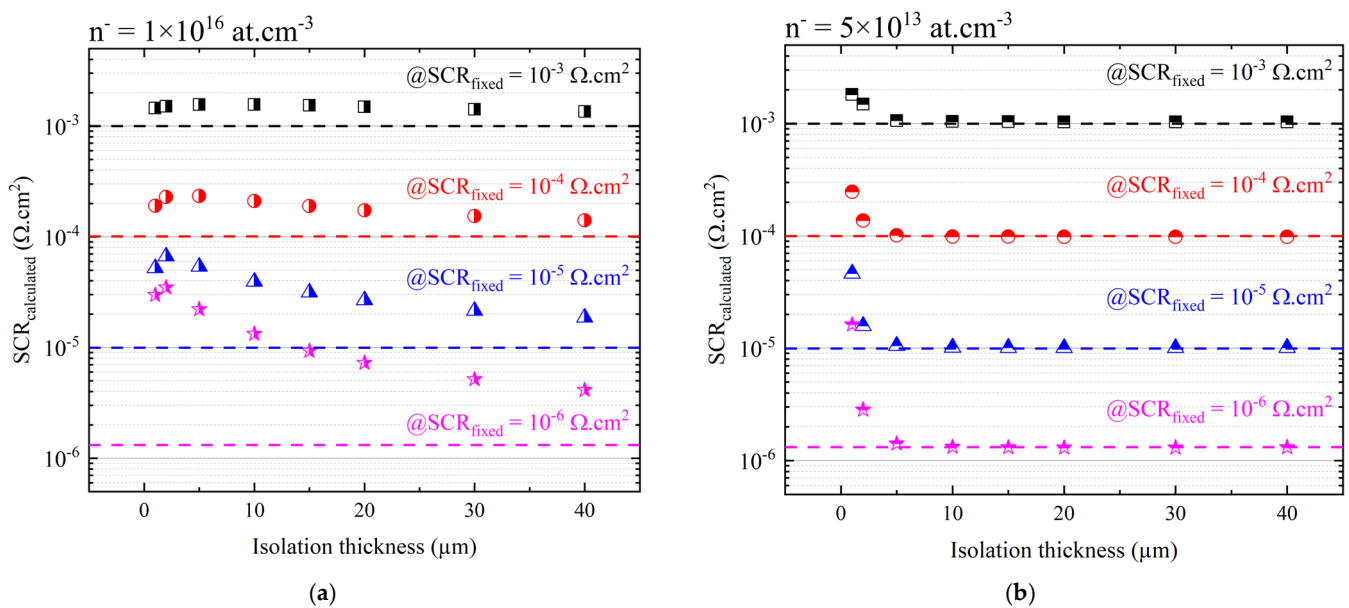


Figure 8. Evolution of the $\text{SCR}_{\text{calculated}}$ for isolation thickness ranging from 1 to $40 \mu\text{m}$ when the doping of the isolation layer is fixed at (a) $1 \times 10^{16} \text{ at}\cdot\text{cm}^{-3}$ and (b) $5 \times 10^{13} \text{ at}\cdot\text{cm}^{-3}$. Dashed lines represent the reference values, taken from Table 1, for a $2 \mu\text{m}$ thick 4H-SiC layer perfectly isolated.

First, no matter the doping level of the isolation, we observe that, independently of the contact performances defined by the $\text{SCR}_{\text{fixed}}$, the increase in the isolation layer thickness tends towards lowering the deviation of the calculated specific contact resistance compared with their reference values. It is even clearer for the good performing contacts ($\text{SCR}_{\text{fixed}} \leq 10^{-5} \Omega\cdot\text{cm}^2$).

Afterwards, as seen in Figure 8a, for an isolation doping level of $1 \times 10^{16} \text{ at}\cdot\text{cm}^{-3}$, the error on the SCR determination (illustrated by the gap between the symbol and the dashed line) seems quite acceptable for the largest thicknesses and for $\text{SCR}_{\text{fixed}} \geq 10^{-4} \Omega\cdot\text{cm}^2$. But, the miscalculation strongly increases for good ohmic contacts presenting a lower $\text{SCR}_{\text{fixed}}$. For instance, at $\text{SCR}_{\text{fixed}} = 10^{-6} \Omega\cdot\text{cm}^2$, the overestimation factor is 5.5 for the $20 \mu\text{m}$ thick isolation layer, which means that the SCR value that could be determined experimentally would be $5.5 \times 10^{-6} \Omega\cdot\text{cm}^2$ whenever the intrinsic SCR level might be $1 \times 10^{-6} \Omega\cdot\text{cm}^2$. Therefore, this isolation doping level seems compatible for measuring low performing contacts reporting SCR up to $10^{-4} \Omega\cdot\text{cm}^2$.

Table 2. Simulated specific contact resistances for several structures with an isolation layer. The symbol “ \triangle ” indicates that $L_T > 25 \mu\text{m}$.

Doping and thickness of the isolation ($\text{at}\cdot\text{cm}^{-3}$) (μm)		$\text{SCR}_{\text{fixed}}$							
		$10^{-3} \Omega\cdot\text{cm}^2$		$10^{-4} \Omega\cdot\text{cm}^2$		$10^{-5} \Omega\cdot\text{cm}^2$		$10^{-6} \Omega\cdot\text{cm}^2$	
		$\text{SCR}_{\text{calculated}}$ ($\times 10^{-3} \Omega\cdot\text{cm}^2$)	\triangle	$\text{SCR}_{\text{calculated}}$ ($\times 10^{-4} \Omega\cdot\text{cm}^2$)	\triangle	$\text{SCR}_{\text{calculated}}$ ($\times 10^{-5} \Omega\cdot\text{cm}^2$)	\triangle	$\text{SCR}_{\text{calculated}}$ ($\times 10^{-6} \Omega\cdot\text{cm}^2$)	\triangle
1×10^{16}	1	1.45	\triangle	1.91	\triangle	5.21	\triangle	29.81	\triangle
	2	1.51	\triangle	2.28	\triangle	6.66	\triangle	34.85	\triangle
	5	1.56	\triangle	2.33	\triangle	5.37	\triangle	22.13	
	10	1.57	\triangle	2.10	\triangle	3.93		13.28	
	20	1.49	\triangle	1.74	\triangle	2.67		7.25	
	40	1.35	\triangle	1.41	\triangle	1.87		4.13	
5×10^{15}	1	1.49	\triangle	2.16	\triangle	6.22	\triangle	33.67	\triangle
	2	1.58	\triangle	2.60	\triangle	6.78	\triangle	30.71	\triangle
	5	1.57	\triangle	2.13	\triangle	4.01		13.60	
	10	1.50	\triangle	1.76	\triangle	2.71		7.33	
	20	1.37	\triangle	1.44	\triangle	1.90		4.12	
	40	1.23	\triangle	1.22		1.45		2.65	
1×10^{15}	1	1.64	\triangle	2.62	\triangle	6.14	\triangle	26.02	
	2	1.80	\triangle	2.33	\triangle	3.68		10.79	
	5	1.35	\triangle	1.39		1.77		3.63	
	10	1.21	\triangle	1.19		1.37		2.32	
	20	1.13	\triangle	1.09		1.18		1.78	
	40	1.08	\triangle	1.03		1.10		1.55	
5×10^{14}	1	1.72	\triangle	2.62	\triangle	5.52	\triangle	21.57	
	2	1.79	\triangle	1.94	\triangle	2.64		6.45	
	5	1.23	\triangle	1.21		1.40		2.41	
	10	1.13	\triangle	1.09		1.18		1.78	
	20	1.08	\triangle	1.03		1.09		1.53	
	40	1.06	\triangle	1.01		1.05		1.42	
1×10^{14}	1	1.80	\triangle	2.50	\triangle	4.74		16.88	
	2	1.55	\triangle	1.44		1.70		3.19	
	5	1.09	\triangle	1.04		1.09		1.52	
	10	1.05	\triangle	1.00		1.04		1.37	
	20	1.04	\triangle	0.99		1.02		1.33	
	40	1.04	\triangle	0.99		1.01		1.32	
5×10^{13}	1	1.82	\triangle	2.48	\triangle	4.63		16.23	
	2	1.49	\triangle	1.37		1.58		2.84	
	5	1.06	\triangle	1.01		1.05		1.41	
	10	1.04	\triangle	0.99		1.02		1.32	
	20	1.04	\triangle	0.98		1.01		1.31	
	40	1.03	\triangle	0.98		1.01		1.31	

On the other hand, as seen in Figure 8b, at the isolation doping level of $5 \times 10^{13} \text{at}\cdot\text{cm}^{-3}$, we observe that the overestimation factor becomes almost non-existent for isolation thicknesses higher than $5 \mu\text{m}$, no matter the contact electrical properties. The overestimation factor is equal to 1.07 in the worst case ($5 \mu\text{m}/\text{SCR}_{\text{fixed}} = 10^{-6} \Omega\cdot\text{cm}^2$). This indicates that a $5 \mu\text{m}$ thick isolated layer, with a nitrogen doping at $5 \times 10^{13} \text{at}\cdot\text{cm}^{-3}$, greatly confines the

current circulation into the upper n^+ layer, as confirmed by the cross-section of the current density, as presented in Figure 9.

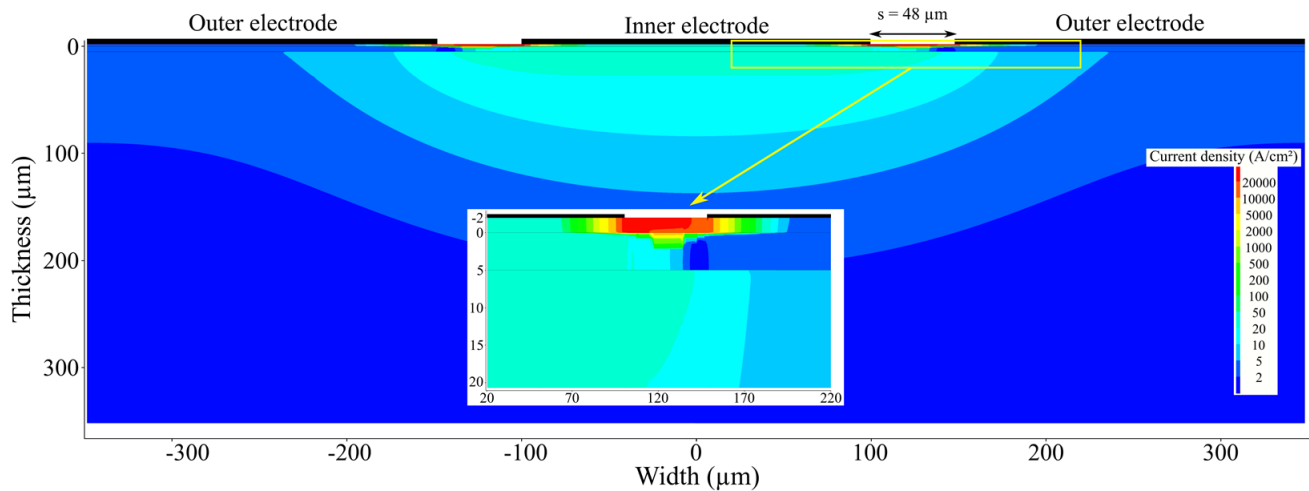


Figure 9. Cross-section of the current density in the c-TLM structure ($s = 48 \mu\text{m}$) when the isolation layer is $5 \mu\text{m}$ thick and doped at $5 \times 10^{13} \text{at}\cdot\text{cm}^{-3}$. The specific contact resistance at the electrode/4H-SiC interface is fixed at $1 \times 10^{-5} \Omega\cdot\text{cm}^2$. An inset picture is presented, highlighting the current density between the electrodes.

6. Experimental Results with $5 \mu\text{m}$ Thick Isolation Layer Doped at $5 \times 10^{13} \text{at}\cdot\text{cm}^{-3}$

Considering these simulation results, we adapted our substrate configuration to experimentally characterize laser-annealed titanium contacts [11]. To do so, we grew an n^- epilayer ($5.6 \mu\text{m}$ thick- $5 \times 10^{13} \text{at}\cdot\text{cm}^{-3}$) onto the Si-face of a production grade 4H-SiC wafer. Then, an n^+ highly nitrogen-doped epilayer ($2.6 \mu\text{m}$ - $1.9 \times 10^{18} \text{at}\cdot\text{cm}^{-3}$) was epitaxied on the top of the isolation layer. Consecutive to the substrate cleaning, a 100nm thick titanium layer was deposited by sputtering. The metal layer was laser-annealed at a fluence of $5.0 \text{J}\cdot\text{cm}^{-2}$. After the irradiation, the patterning of c-TLM was performed thanks to ion beam etching. Finally, a 300nm thick aluminum layer was deposited onto c-TLM structures to thicken the contact.

Figure 10a presents the I-V measurements of a Ti/4H-SiC laser annealed at a fluence of $5.0 \text{J}\cdot\text{cm}^{-2}$. The characteristics are linear, which reveals the ohmic behavior of this Ti contact. Figure 10b shows the evolution of the corrected resistance of c-TLM structures as a function of their spacing. Contrary to the results obtained from the bulk configuration, as presented in Figure 2, the resistance level massively increases. This is attributed to the R_{sh} increasing due to the current confinement near the electrodes. Also, a good correlation level is observed ($R^2 \approx 1$) between the resistance and the measured c-TLM spacing, which allows to reliably evaluate the specific contact resistance at $1 \times 10^{-4} \Omega\cdot\text{cm}^2$.

Using the same substrate configuration, we also performed some experiments using nickel [27]. A laser irradiation with a fluence of $4.75 \text{J}\cdot\text{cm}^{-2}$ led to a reliable extraction of the specific contact resistance, evaluated at $2.4 \times 10^{-5} \Omega\cdot\text{cm}^2$. This result, which is the lowest ever published in the literature using room temperature laser annealing, also highlights that this substrate configuration allows to determine specific contact resistance in the range of $1 \times 10^{-5} \Omega\cdot\text{cm}^2$.

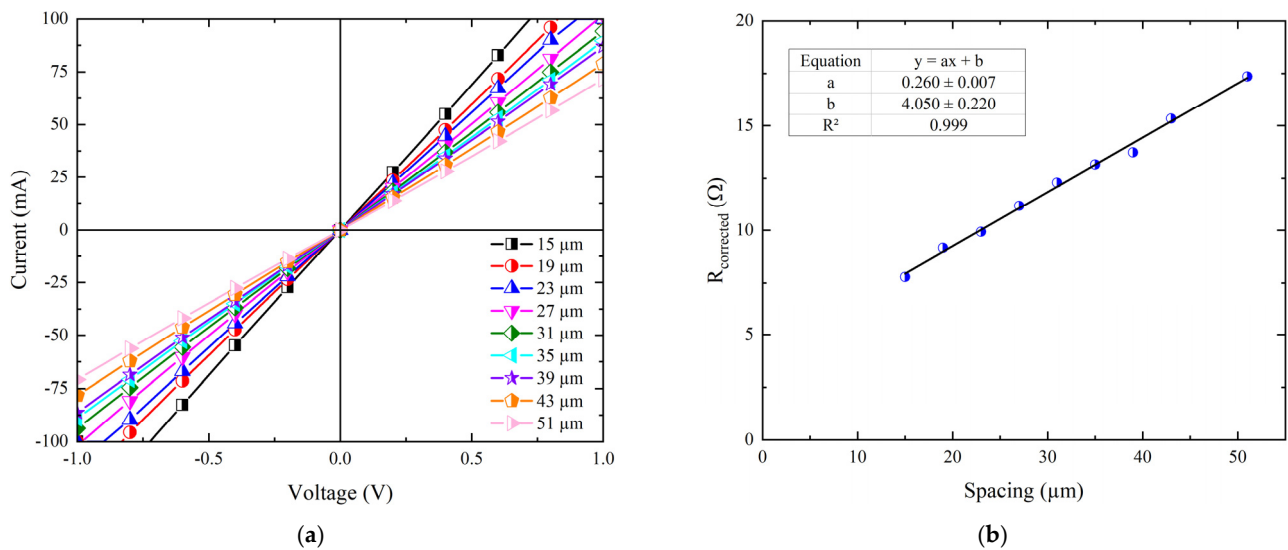


Figure 10. (a) I-V characteristics of a Ti/4H-SiC contact laser annealed at $5.0 \text{ J}\cdot\text{cm}^{-2}$. (b) Evolution of the corrected resistance for the associated Ti/4H-SiC contact.

7. Conclusions

In this work, we simulated c-TLM measurements for ohmic contacts on 4H-SiC presenting specific contact resistances ranging from 1×10^{-3} to $1 \times 10^{-6} \Omega\cdot\text{cm}^2$. It was demonstrated that the substrate configuration can significantly affect the current distribution, which impacts the evaluation of specific contact resistances independently of the intrinsic electrical properties of the contact itself. Although most of the studies used a configuration where contacts were directly achieved on 4H-SiC wafers, it represented the most unfavorable scenario to accurately evaluate the SCR due to a deep current circulation in the SiC substrate. Therefore, we focused on configurations composed of a thin $2 \mu\text{m}$ thick 4H-SiC layer deposited on an isolation layer, itself grown onto the substrate. Both the thickness increase and the doping level lessening of the isolation layer tended towards reducing the misestimation of the SCR. This improvement came from the better current confinement near the electrodes. To accurately determine the electrical properties of good ohmic contacts ($\text{SCR} \leq 1 \times 10^{-5} \Omega\cdot\text{cm}^2$), the need for an efficient isolation was even more required. Based on our results, we evidenced that a $5 \mu\text{m}$ thick isolation layer nitrogen doped at $5 \times 10^{13} \text{ at}\cdot\text{cm}^{-3}$ allowed to accurately determine specific contact resistance values as low as $1 \times 10^{-6} \Omega\cdot\text{cm}^2$.

Author Contributions: Conceptualization, C.B. and J.-F.M.; software, C.B.; investigation, C.B. and J.-F.M.; writing—original draft preparation, C.B.; writing—review and editing, J.-F.M. and D.A.; supervision, J.-F.M. and D.A.; project administration, J.-F.M.; funding acquisition, D.A. All authors have read and agreed to the published version of the manuscript.

Funding: This work was carried out in the framework of the ECSEL JU project WInSiC4AP (Wide Band Gap Innovative SiC for Advanced Power), grant agreement no. 737483.

Data Availability Statement: Data will be made available on request.

Conflicts of Interest: The authors declare no conflicts of interest.

References

1. Crofton, J.; Porter, L.M.; Williams, J.R. The Physics of Ohmic Contacts to SiC. *Phys. Status Solidi B* **1997**, *202*, 581–603. [[CrossRef](#)]
2. Chang, S.-C.; Wang, S.-J.; Uang, K.-M.; Liou, B.-W. Investigation of Au/Ti/Al Ohmic Contact to N-Type 4H-SiC. *Solid State Electron.* **2005**, *49*, 1937–1941. [[CrossRef](#)]
3. Ghandi, R.; Lee, H.S.; Domeij, M.; Zetterling, C.M.; Östling, M. Backside Nickel Based Ohmic Contacts to N-Type Silicon Carbide. *Mater. Sci. Forum* **2008**, *600–603*, 635–638. [[CrossRef](#)]

4. Han, L.; Shen, H.; Liu, K.; Wang, Y.; Tang, Y.; Bai, Y.; Xu, H.; Wu, Y.; Liu, X. Improved Adhesion and Interface Ohmic Contact on N-Type 4H-SiC Substrate by Using Ni/Ti/Ni. *J. Semicond.* **2014**, *35*, 072003. [\[CrossRef\]](#)
5. Ito, K.; Onishi, T.; Takeda, H.; Kohama, K.; Tsukimoto, S.; Konno, M.; Suzuki, Y.; Murakami, M. Simultaneous Formation of Ni/Al Ohmic Contacts to Both n- and p-Type 4H-SiC. *J. Electron. Mater.* **2008**, *37*, 1674–1680. [\[CrossRef\]](#)
6. Cho, N.-I.; Jung, K.-H.; Choi, Y. Improved Ohmic Contact to the N-Type 4H-SiC Semiconductor Using Cobalt Silicides. *Semicond. Sci. Technol.* **2004**, *19*, 306–310. [\[CrossRef\]](#)
7. Rupp, R.; Kern, R.; Gerlach, R. Laser Backside Contact Annealing of SiC Power Devices: A Prerequisite for SiC Thin Wafer Technology. In Proceedings of the 2013 25th International Symposium on Power Semiconductor Devices & IC's (ISPSD), Kanazawa, Japan, 26–30 May 2013; pp. 51–54.
8. Berger, C.; Michaud, J.F.; Chouteau, D.; Alquier, D. Laser Annealing Simulations of Metallisations Deposited on 4H-SiC. *Mater. Sci. Forum* **2019**, *963*, 502–505. [\[CrossRef\]](#)
9. Ding, J.; Li, X.; Yang, K.; Zhu, Y. Numerical Simulation on Controlling the Front-Side Temperature of Thinned SiC Substrate during Ohmic Contact to Ni or Ti Using Back-Side Laser Annealing. *J. Appl. Phys.* **2022**, *132*, 035703. [\[CrossRef\]](#)
10. De Silva, M.; Kawasaki, T.; Miyazaki, T.; Koganezawa, T.; Yasuno, S.; Kuroki, S.-I. Formation of Epitaxial Ti-Si-C Ohmic Contact on 4H-SiC C Face Using Pulsed-Laser Annealing. *Appl. Phys. Lett.* **2017**, *110*, 252108. [\[CrossRef\]](#)
11. Berger, C.; Alquier, D.; Bah, M.; Michaud, J.-F. Electrical, Morphological and Structural Properties of Ti Ohmic Contacts Formed on n-Type 4H-SiC by Laser Thermal Annealing. *Mater. Sci. Semicond.* **2022**, *151*, 106983. [\[CrossRef\]](#)
12. Rascunà, S.; Badalà, P.; Tringali, C.; Bongiorno, C.; Smecca, E.; Alberti, A.; Di Franco, S.; Giannazzo, F.; Greco, G.; Roccaforte, F.; et al. Morphological and Electrical Properties of Nickel Based Ohmic Contacts Formed by Laser Annealing Process on N-Type 4H-SiC. *Mater. Sci. Semicond.* **2019**, *97*, 62–66. [\[CrossRef\]](#)
13. Badalà, P.; Deretzis, I.; Sanzaro, S.; Pennisi, F.M.; Bongiorno, C.; Fiscaro, G.; Rascunà, S.; Bellocchi, G.; Bassi, A.; Boscaglia, M.; et al. Ni-Silicide Ohmic Contacts on 4H-SiC Formed by Multi Pulse Excimer Laser Annealing. *Solid State Phenom.* **2023**, *344*, 15–22. [\[CrossRef\]](#)
14. Zhou, Z.; He, W.; Zhang, Z.; Sun, J.; Schöner, A.; Zheng, Z. Characteristics of Ni-Based Ohmic Contacts on n-Type 4H-SiC Using Different Annealing Methods. *Nanotechnol. Precis. Eng.* **2021**, *4*, 013006. [\[CrossRef\]](#)
15. Cheng, Y.; Lu, W.; Wang, T.; Chen, Z. Fabrication of Ohmic Contact on Semi-Insulating 4H-SiC Substrate by Laser Thermal Annealing. *J. Appl. Phys.* **2016**, *119*, 225705. [\[CrossRef\]](#)
16. Schroder, D.K. *Semiconductor Material and Device Characterization*, 3rd ed.; John Wiley & Sons: Hoboken, NJ, USA, 2006; ISBN 978-0-471-73906-7.
17. Cao, Y.; Perez-Garcia, S.A.; Nyborg, L. Investigation of Ni/Ta Contacts on 4H Silicon Carbide upon Thermal Annealing. *Appl. Surf. Sci.* **2007**, *254*, 139–142. [\[CrossRef\]](#)
18. Kuchuk, A.; Kladko, V.; Guziewicz, M.; Piotrowska, A.; Minikayev, R.; Stonert, A.; Ratajczak, R. Fabrication and Characterization of Nickel Silicide Ohmic Contacts to N-Type 4H Silicon Carbide. *J. Phys. Conf. Ser.* **2008**, *100*, 042003. [\[CrossRef\]](#)
19. Jiang, S.-Y.; Li, X.-Y.; Chen, Z.-Z. Role of W in W/Ni Bilayer Ohmic Contact to n-Type 4H-SiC from the Perspective of Device Applications. *IEEE Trans. Electron. Devices* **2018**, *65*, 641–647. [\[CrossRef\]](#)
20. Wang, Z.; Liu, W.; Wang, C. Recent Progress in Ohmic Contacts to Silicon Carbide for High-Temperature Applications. *J. Electron. Mater.* **2016**, *45*, 267–284. [\[CrossRef\]](#)
21. Roccaforte, F.; La Via, F.; Raineri, V. Ohmic contacts to SiC. *Int. J. High Speed Electron. Syst.* **2005**, *15*, 781–820. [\[CrossRef\]](#)
22. Rideout, V.L. A Review of the Theory, Technology and Applications of Metal-Semiconductor Rectifiers. *Thin Solid Film.* **1978**, *48*, 261–291. [\[CrossRef\]](#)
23. Kawahara, K.; Suda, J.; Pensl, G.; Kimoto, T. Reduction of Deep Levels Generated by Ion Implantation into N- and p-Type 4H-SiC. *J. Appl. Phys.* **2010**, *108*, 033706. [\[CrossRef\]](#)
24. Michaud, J.F.; Song, X.; Biscarrat, J.; Cayrel, F.; Collard, E.; Alquier, D. Aluminum Implantation in 4H-SiC: Physical and Electrical Properties. *Mater. Sci. Forum* **2012**, *740–742*, 581–584. [\[CrossRef\]](#)
25. Han, S.Y.; Kim, K.H.; Kim, J.K.; Jang, H.W.; Lee, K.H.; Kim, N.-K.; Kim, E.D.; Lee, J.-L. Ohmic Contact Formation Mechanism of Ni on n-Type 4H-SiC. *Appl. Phys. Lett.* **2001**, *79*, 1816–1818. [\[CrossRef\]](#)
26. Klootwijk, J.H.; Timmering, C.E. Merits and Limitations of Circular TLM Structures for Contact Resistance Determination for Novel 111-V HBTs. In Proceedings of the 2004 International Conference on Microelectronic Test Structures (IEEE Cat. No. 04CH37516), Awaji, Japan, 22–25 March 2004.
27. Michaud, J.F.; Berger, C.; Alquier, D. Nickel Ohmic Contacts Formed on 4H-SiC by UV Laser Annealing. In Proceedings of the International Conference on Silicon Carbide and Related Materials (ICSCRM), Sorrento, Italy, 17–22 September 2023.

Disclaimer/Publisher's Note: The statements, opinions and data contained in all publications are solely those of the individual author(s) and contributor(s) and not of MDPI and/or the editor(s). MDPI and/or the editor(s) disclaim responsibility for any injury to people or property resulting from any ideas, methods, instructions or products referred to in the content.